Biomineralization Mechanism of Gold by Zygomycete Fungi Rhizopous oryzae

Sujoy K. Das,[†,⊥,*] Jinni Liang,[†] Michael Schmidt,[‡] Fathima Laffir,[§] and Enrico Marsili[†,*]

[†]School of Biotechnology, National Centre for Sensor Research, Dublin City University, Dublin 9, Ireland, [‡]Tyndall National Institute, Cork, Ireland, and [§]Materials and Surface Science Institute, University of Limerick, Limerick, Ireland. [⊥]Present address: Environmental Technology Laboratory, Central Leather Research Institute (CLRI)-Council of Scientific and Industrial Research (CSIR), Chennai, India.

ABSTRACT

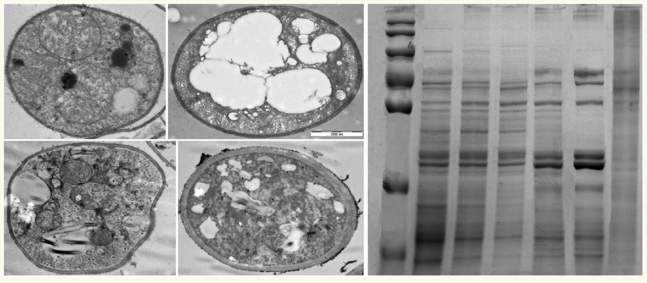

In recent years, there has been significant progress in the biological synthesis of nanomaterials. However, the molecular mechanism of gold biomineralization in microorganisms of industrial relevance remains largely unexplored. Here we describe the biosynthesis mechanism of gold nanoparticles (AuNPs) in the fungus *Rhizopus oryzae*. Reduction of $AuCl_4^-$ [Au(III)] to nanoparticulate Au^0 (AuNPs) occurs in both the cell wall and cytoplasmic region of *R. oryzae*. The average size of the as-synthesized AuNPs is ~15 nm. The biomineralization occurs through adsorption, initial reduction to Au(I), followed by complexation [Au(I) complexes], and final reduction to Au^0. Subtoxic concentrations (up to 130 μM) of $AuCl_4^-$ in the growth medium increase growth of *R. oryzae* and induce two stress response proteins while simultaneously down-regulating two other proteins. The induction increases mycelial growth, protein yield, and AuNP biosynthesis. At higher Au(III) concentrations (>130 μM), both mycelial and protein yield decrease and damages to the cellular ultrastructure are observed, likely due to the toxic effect of Au(III). Protein profile analysis also confirms the gold toxicity on *R. oryzae* at high concentrations. Sodium dodecyl sulfate polyacrylamide gel electrophoresis analysis shows that two proteins of 45 and 42 kDa participate in gold reduction, while an 80 kDa protein serves as a capping agent in AuNP biosynthesis.

KEYWORDS: gold nanoparticles · biomineralization · bioconjugate · biosynthetic mechanism · stress response proteins

Metallic nanoparticles (MNPs) have been synthesized utilizing various physical and chemical methodologies.[1−3] However, there is a growing demand to develop clean, nontoxic, and environmentally benign synthetic technologies for nanoparticle production. Biosynthetic protocols are receiving increasing attention because of the milder process condition, absence of toxic chemicals, and well-focused distribution of the produced nanoparticles.[4−8] In nature, biological systems developed biomineralization processes to nucleate, grow, and assemble inorganic materials such as gypsum, calcite, magnetite, silicates, *etc.*[9−11] The specific interactions involving proteins and inorganic compounds during the growth process govern the shape and crystal structure of biominerals along with their assembly behavior.[12,13] The role of microbes in metal biogeochemistry was discovered more than 35 years ago, and the concept of microbial nanofactories, that is, viable microorganisms for nanostructure fabrication, has been proposed for various applications.[14−16] Precious metal nanoparticles were the first nanostructures to be considered, in view of their high value and their relevance to the mining industry.[17,18]

Among other MNPs, gold nanoparticles (AuNPs) offer scope for biomedical and environmental applications because of pronounced biocompatibility, chemical inertness, and characteristic optoelectronic properties.[19−21] Therefore, biosynthetic protocols for AuNP production are of paramount importance. A number of microorganisms such as bacteria,[8,22−24] fungi,[8,25,26] yeast,[12,27,28] and viruses[29,30] have been explored for MNP synthesis. In their pioneer work, Klaus *et al.*[22] demonstrated intracellular synthesis of silver nanoparticles (AgNPs) using *Pseudomonas stutzeri* AG259. Lengke and coworkers[24] proposed synthesis of AuNPs through incubation of gold(I)−thiosulfate and gold(III)−chloride complexes with filamentous cyanobacteria, while Reith *et al.*[31,32] recently reported formation of AuNPs by gram-negative β-proteobacteria *Cupriavidus metallidurans* and *Ralstonia* sp.

While the formation mechanism of AuNPs by prokaryotes is understood to some extent, the AuNP biosynthesis in viable fungi is a relatively recent discovery. Only few

* Address correspondence to sujoydasiacs@gmail.com, enrico.marsili@dcu.ie.

Received for review April 5, 2012 and accepted June 18, 2012.

Published online June 18, 2012
10.1021/nn301502s

species such as *Verticillium*, *Phoma* sp., *Rhizopus oryzae*, *Fusarium oxysporum*, *Aspergillus fumigatus*, and *Trichoderma asperellum* have been investigated.[25,26,33] Extracellular synthesis of AuNPs has been reported using *Trichodermaviride*, while *Verticillium* sp. produced AuNPs in an intracellular organelle.[25,33] Among other fungi, *R. oryzae* possesses several advantages as a microbial nanofactory: (1) large quantity of viable mycelia are obtained by growing the fungus in easily available and low-cost growth medium; (2) downstream processing and handling of *R. oryzae* mycelia is less complex than bacteria and viruses; (3) *R. oryzae* is nonpathogenic and does not require special biosafety measures; (4) it produces a significant quantity of proteins; and (5) nearly monodisperse, water-soluble nanoparticles are obtained in the biosynthesis process.[33−35] Because of these positive characteristics, we investigate here the biosynthetic route of AuNPs in *R. oryzae*. To enhance the applicability of this fungus in nanoparticle synthesis and increase the synthesis rate, as well, it is important to understand the biochemical and molecular mechanism involved in the process. In addition, in-depth knowledge of biomineralization mechanisms is required to control the size, shape, and crystallinity of biosynthetic nanoparticles.

Microorganisms possess a diverse range of mechanism for reduction and biomineralization of metal ions.[9,33,36−43] For example, certain dissimilatory reducing bacteria (*Geobacter*, *Shewanella*, *Desulfovibrio*, *etc.*) use outer membrane cytochromes,[36−38] while others use various reductases.[36,39] Enzyme-catalyzed formation of AuNPs have been described in bacteria and archea,[41−43] while Checa *et al.*[44] reported that a Au-specific efflux system is involved in the Au biomineralization in *Salmonella enterica*. Furthermore, the biosynthetic mechanisms are distinguished according to the location of AuNP formation, that is, cytoplasm, the periplasm, or in the extracellular space.[25,33] Therefore, the understanding of fundamental molecular mechanism, interaction of Au ions with the organism, and the response to Au toxicity are necessary for the development of an industrial bioprocess for AuNP synthesis employing *R. oryzae*. This study deals with the interaction of $HAuCl_4$ with viable zygomycete fungi *R. oryzae*, the distribution and speciation of Au in the cells, and the genetic/biochemical response of the microorganism. Our results will help to develop a large-scale bioprocess for AuNP synthesis, thus reducing the cost and environmental impact of the nanoparticles industry.

RESULTS AND DISCUSSION

Synthesis of AuNPs by *R. oryzae*. Incubation of *R. oryzae* mycelia with $HAuCl_4$ solution results in gradual color change of the mycelia with time from pale white to purple (Figure 1A). After 48 h, the UV−vis spectrum of the purple mycelia showed a peak at 535 nm

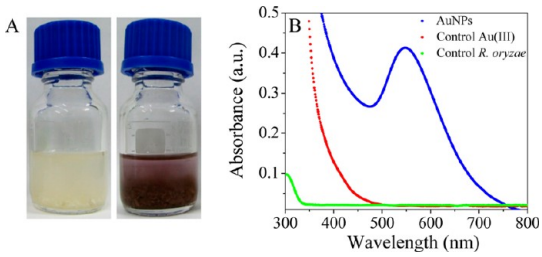

Figure 1. Photographs (A) of control and AuNP-synthesized *R. oryzae* mycelia after 48 h incubation; UV-vis spectra (B) of the dispersed AuNPs, $HAuCl_4$ solution, and control *R. oryzae* mycelia.

(Figure 1B), indicating the formation of AuNPs. The absorption band at 535 nm is due to the surface plasmon resonance (SPR) of AuNPs,[7] which indicates bioreduction of Au(III) to Au^0. Solution without mycelium did not change color.

The process was repeated at pH between 3.0 and 10.0 to understand the interaction of Au(III) with *R. oryzae*. At low (<4.0) pH, the reaction was completed within 12 h, while at high pH (>8.0), it took 72 h. The protonation of surface functional groups at low pH results in an overall positive charge, which facilitates the electrostatically driven sorption of negatively charged $AuCl_4^-$ [Au(III)] ions.[45] Zeta-potential of *R. oryzae* showed that at low pH the cell surface carries net positive charge.[46] Therefore, pH-driven AuNP formation could be explained by electrostatic interaction of positively charged cell wall functional groups and negatively charged Au(III) ions followed by reduction to AuNPs. Scanning electron microscope (SEM) images show formation of AuNPs on the mycelia surface, suggesting mycelia acts as a template in the AuNP synthesis. On the mycelia surface, AuNPs appeared as bright dots (Figure 2A), which is more evident in the high-magnification image (Figure 2B and Supporting Information Figure S1), due to their electron dense metallic character. Area profile energy-dispersive X-ray analysis (EDXA) of the mycelia after AuNP synthesis shows the appearance of Au peaks along with C, N, O, K, and Cu peaks (Figure 2C). The Au peaks correspond to the formation of AuNPs, and Cu peaks are coming from the copper stub, whereas C, N, O, and K arise from X-ray emission of proteins and carbohydrate on the mycelia surface, indicating that AuNP formation and conjugation occur in close proximity of the mycelia surface.

Transmission electron micrographs (TEM) show AuNPs on the cell wall as well as in the cytoplasmic region (Figure 2D−F), indicating that Au(III) reduction to Au^0 occurs in both cell locations. Quantitative elemental analysis data (Supporting Information, Table S1) show that the number of AuNPs per unit area is higher in the cytoplasmic regions than on the cell wall. The multiple spectra were recorded from different regions of the cell wall and cytoplasm. The quantitative

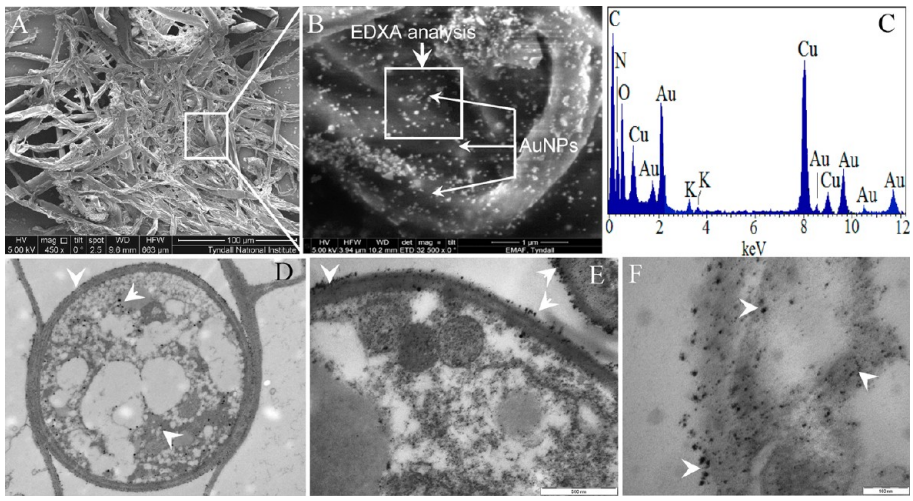

Figure 2. SEM micrographs at low (A) and high (B) magnification of *R. oryzae* incubated with Au(III) at 30 °C for 48 h. EDX analysis (C) confirms AuNP formation. TEM micrograph of *R. oryzae* (D) shows formation of AuNPs following interaction with Au(III) at 30 °C for 48 h. HRTEM images confirm that AuNPs form in the cell wall (E) and cytoplasmic (F) regions.

elemental analysis was calculated from the mean value derived from those multiple spectra, and the squared deviation was approximately 5%. Considerable difference in Au quantity in the cell wall and cytoplasmic region suggests that a major amount of Au(III) is transported into the cytoplasm and then undergoes protein-mediated bioreduction to form AuNPs.

The protein-mediated reduction in the cytoplasm was confirmed by synthesis of AuNPs using cell-free protein extract (see Experimental Section). Results show that Au(III) reductions to Au^0 occur both in crude cell-free protein extract and partially purified cytoplasmic protein(s), as shown by the appearance of the SPR band at 535 nm. High-resolution transmission electron microscopic (HRTEM) (Supporting Information, Figure S2A,B) image shows formation of 15.9 ± 2.8 nm AuNPs by partially purified cytoplasmic protein(s). The EDXA spectrum (Supporting Information, Figure S2C) shows Au peaks along with C, N, O, and K peaks resulting from conjugation of protein(s) on the AuNP surface. The Cu peaks in the spectrum originated from the copper grid. Selected area electron diffraction (SAED) (Supporting Information, Figure S2D) of AuNPs shows the Scherrer ring patterns associated with the [111], [200], [222], and [311] atomic planes of Au (JCPDS, No. 04-0784) and indicated the formation of a face-centered cubic (fcc) crystal lattice.[7,47]

Au speciation in the biomineralization process was further studied through X-ray photoelectron spectroscopy (XPS) technique. Consistently with the general biochemical composition of fungal cell wall, C_{1s}, N_{1s}, O_{1s}, and P_{2p} peaks were observed in both mycelia (Supporting Information, Figure S3A). However, an additional peak of Au_{4f} was noted on the mycelia following mineralization of gold ions (Supporting Information, Figure S3B). The core-level spectra of C_{1s}, N_{1s}, O_{1s}, and P_{2p} for control mycelia (Supporting Information, Figure S4A–D) demonstrated that different cell surface functional groups like carboxyl, amine, phosphate, *etc.* provide Au(III) binding sites for mineralization of Au. Following interaction with Au(III) ions, XPS spectra of mycelia showed a shift of C_{1s} and N_{1s} peaks to higher binding energy (Figure 3A–D), compared to the control mycelia. Further, high binding energy peaks for carboxylate and protonated amine or amide groups disappeared following interaction with Au(III) ions, suggesting gold ions were complexed with the carboxyl and amine groups of phosphoproteins present on the cell surface. The related Au_{4f} spectrum collected from the mycelia at different time intervals (24 and 48 h) was composed of doublet peaks, which could both be assigned to Au^0.[48,49] The asymmetry in the peaks could be resolved to describe an additional chemical state, which was attributed to Au(I).[48,49] Interestingly, the concentration of Au(I) is higher in the mycelium harvested at 24 h than at 48 h (Figure 3F), indicating the formation of AuNPs through intermediate Au(I) species. However, the reduction of Au(I) species to AuNPs does not cause any shifting of core-level C_{1s}, N_{1s}, O_{1s}, and P_{2p} spectra with time. The XPS results strongly suggest that Au(III) was rapidly reduced to Au(I) species upon initial binding on the mycelia by electrostatic or covalent interaction, and then further slowly reduced to Au^0. The formation of Au(I) species suggests the possibility of Au methylation as an additional detoxification mechanism.[50,51] Methylation of metals (*e.g.*, Hg, Bi, Tn, or Ge) have been reported in several microorganisms[51] as a defense mechanism and have been involved in Au biomineralization in *R. oryzae*.

The interaction of Au(III) with protein was also studied by XPS analysis. Similar spectra of C_{1s}, O_{1s}, N_{1s}, P_{2p}, and Au_{4f} to that of the Au–mycelia interaction were observed following interaction of Au(III) with the partially purified protein extract. The doublet peaks of

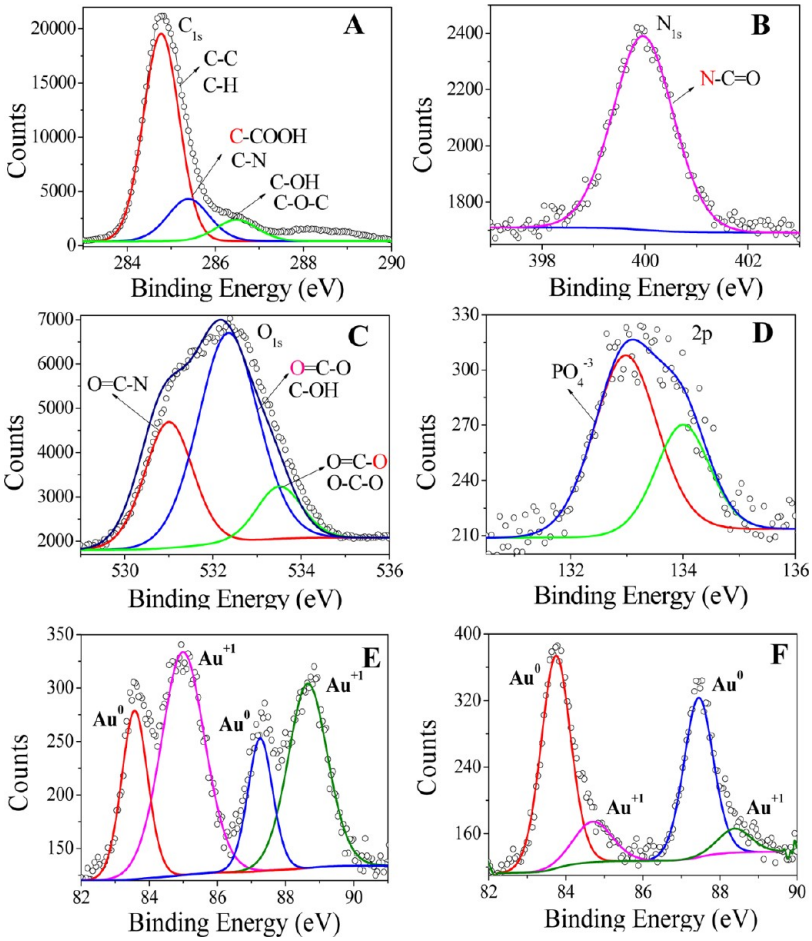

Figure 3. XPS spectra of the *R. oryzae* mycelia showing the core-level C_{1s} (A), N_{1s} (B), O_{1s} (C), P_{2p} (D), and Au_{4f} after 24 h (E) and 48 h (F) reaction with gold ions. The intensity of the core-level Au(I) peak is higher in the mycelium harvested at 24 h compared to Au^0. The core-level Au(I) and Au^0 peaks decrease and increase with time, respectively.

$4f_{7/2}$ and $4f_{5/2}$, which correspond to Au^0,[48,49] were observed after AuNP synthesis (48 h). The binding energies for Au(I) were observed after 24 h, that is, before the completion of the AuNP biosynthesis process. The changes of Au(I) and Au^0 peaks with time suggest that formation of AuNPs by protein extract occurs through a similar pathway to those of the mycelia surface. The core-level spectra of C_{1s}, N_{1s}, O_{1s}, and P_{2p} in the control protein extract were observed at the same positions as described for the mycelia. The shifts of C_{1s} and N_{1s} peaks to higher energy with respect to cell-free protein extract following interaction with Au(III) ions suggest that conjugation of protein with AuNPs occurs in the reduction process. The negative surface charge (ζ value of -24.8 ± 1.2 mV) of protein extract showed that Au(III) ions bind with cytosolic protein(s) through covalent interaction instead of electrostatic interaction. This result further demonstrates that gold ions interacted with protein molecules and get reduced to AuNPs. The zeta-potential (ζ) of the biosynthetic AuNPs was -25.5 mV. The protein molecules acted as both reducing and capping agents. Conjugation of protein with AuNPs is responsible for negative ζ value and gives stability to the synthesized AuNPs.

Metabolism of Gold by *R. oryzae*. Metabolism of gold in *R. oryzae* was evaluated by growing the mycelia in the presence of gold ions. The growth curves of *R. oryzae* at various Au(III) concentrations (0–400 μM) are shown in Figure 4. At low Au(III) concentration (<130 μM), the growth rates and mycelial yields of *R. oryzae* at early stationary phase (72 h) increased from 265 mg/100 mL without Au(III) to 329 mg/100 mL, while the lag phase decreased from 18 to 9 h (Figure 4A). However, at higher Au(III) concentrations (400 μM) resulted in lower mycelial yield and increased lag phase: 226 mg/100 mL and 32 h, respectively.

The effect of Au(III) in the metabolism of *R. oryzae* was further studied by measuring the total protein concentration in the mycelia. The total protein concentration after 72 h of growth (Figure 4B) showed similar trend to that of mycelial yields, with a maximum of 14.3 mg/mL at 130 μM Au(III). The control mycelia have a protein concentration of 7.25 mg/mL. Thus, Au(III) has a strong impact on cellular growth and protein expressions and becomes toxic at a concentration higher

than 130 μM. At low concentration, *R. oryzae* respond by increasing proteins expression, including those responsible for gold bioreduction and detoxification. At higher Au(III) concentrations, the detoxification mechanism(s) are not sufficient to maintain the cellular integrity due to toxic effect of gold ions. TEM micrographs showed that Au(III) ions had no impact on the cellular ultrastructure up to 130 μM (Figure 5A,B); however, significant structural alterations of the cell were noticed following growth in the presence of higher Au(III) concentration (250 μM $AuCl_4^-$). This results in cell elongation, aggregation of cytoplasmic content, and enlargement of the cell vacuoles (Figure 5C). The elongation of the cells caused a decrease in surface/volume ratio. The ultrastructure changes were due to the toxic effect of Au(III) at this concentration. The cell wall also became thicker, suggesting that the cell wall acted as a permission barrier against metal toxicity. Alteration of surface morphology under stress condition has been reported as a defense mechanism.[52,53] This confirms that Au(III) has a significant impact on cellular response.

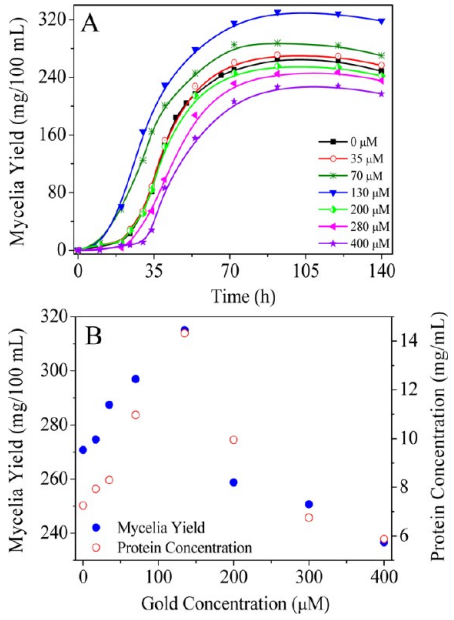

Figure 4. Growth kinetics of (A) *R. oryzae* grown with 0 to 400 μM Au(III) in the medium. Correlation between protein and mycelia yield (B) with Au(III) ion concentration in the medium during growth of *R. oryzae*.

Inducible expression of protein(s) in *R. oryzae* was then studied by sodium dodecyl sulfate polyacrylamide gel electrophoresis (SDS-PAGE) (Figure 5E) to assess the cellular response on low (15 and 35 μM), medium (70 and 130 μM), and high (250 μM) Au(III) concentration. Both up- and down-regulation of proteins was observed in the presence of Au(III). Two proteins with MW ~45 and ~42 kDa were up-regulated in the cells grown in the presence of 70−130 μM Au(III) (Figure 5E, lanes 5 and 6), at the same time, two other proteins with MW of ~68 and ~50 kDa were also suppressed (Figure 5E, lanes 2 and 3). Expression of ~45 and ~42 kDa proteins increased, while that of ~68 and ~50 kDa proteins decreased with increasing Au(III) concentrations, showing concentration-dependent protein expression. However, in the presence of a high amount of Au(III) (250 μM), protein expressions were suppressed due to the toxic effect of Au(III). Results suggest that Au(III) might play a role in the expression of an oxidative stress response gene, which up-regulated oxido-reductase enzymes.[54] Further, *R. oryzae* responds with concentration-dependent active biochemical detoxification when exposed to Au(III) ions.

Reith *et al.*[31] recently observed up-regulation of several oxidative stress response genes in *Cupriavidus metallidurans* grown in the presence of Au(III). Au-dependent and Au-specific regulation has been reported in *Escherichia coli* despite Au being a rare, inert, and non-essential metal.[55] Nonspecific regulation of CueR, a MerR-like transcriptional activator, which usually responds to Cu(II), was activated by Au(III)

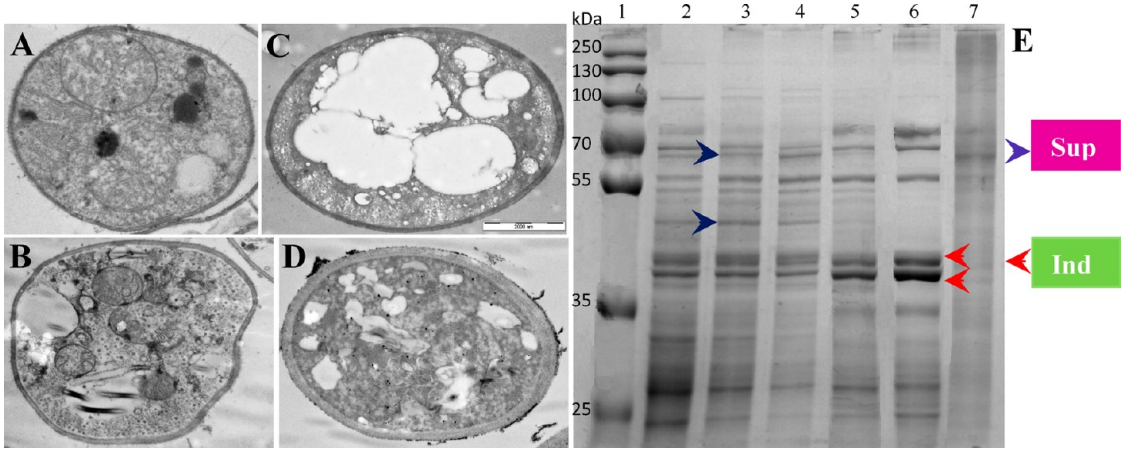

Figure 5. TEM micrographs of the *R. oryzae* ultrastructure grown in the presence of 0 μM (A), 130 μM (B), and 250 μM of Au(III) (C). TEM micrograph of the mycelia grown in the presence of 130 μM Au(III), after AuNP synthesis shows enhanced AuNP synthesis due to inducible expression of proteins (D). SDS-PAGE of whole proteins following growth in the presence of 0 (lane 2), 15 (lane 3), 35 (lane 4), 70 (lane 5), 130 (lane 6), and 250 μM (lane 7) of Au(III) (E). Arrows indicate suppressed and induced proteins.

complexes.[55] This activation was promoted by binding of Au(III) to the cysteine (Cys) residues 112 and 120. Checa *et al.*[44] also characterized a transcriptional regulator (GolS) in Au(III)-resistant *Salmonella enterica*. Expression of transmembrane efflux ATPase (GolT) and metallochaperone (GolB) genes were activated by GolS. A further GolS-regulated locus *gesABC* for GolS-induced CBA (consisting of subunits C, B, and A) efflux system-coding operon has been recently described in Au(III)-resistant *Salmonella* strains; *gesABC* is a *Salmonella*-specific CBA efflux system required for Au(III) resistance in this bacterium.[44,56]

The role of Au(III)-induced proteins in Au mineralization was further investigated to determine the biomineralization mechanism. *R. oryzae* mycelia grown with Au(III) were incubated with Au(III), and formation of AuNPs was studied as described above. TEM micrograph demonstrated that more AuNPs were accumulated or synthesized in both the cell wall and cytoplasmic regions of *R. oryzae* grown in the presence of 130 μM Au(III) (Figure 5D and Supporting Information, Figure S5) compared to the control mycelia (Figure 2D–F). However, formation of AuNPs was inhibited in *R. oryzae* grown in the presence of 250 μM Au(III) (Supporting Information, Figure S6), as the toxic effect of Au(III) at higher concentration suppressed expression of proteins (Figure 5E, lane 7), and thus AuNP synthesis was inhibited. On the other hand, in the presence of 130 μM Au(III), the induced proteins (Figure 5E, lane 6), most probably metal reductase proteins, enhanced AuNP synthesis.

Finally, the role of these Au(III)-inducible expressed proteins in AuNP biosynthesis was evaluated by interaction of Au with protein extract. The protein extracts were prepared from *R. oryzae* mycelia grown in the presence of different concentrations of Au(III) and used in AuNP synthesis. The rate of AuNP synthesis was higher in protein extract prepared from mycelia grown with Au(III) up to 130 μM compared with control one (Supporting Information, Figure S7). At the latter Au(III) concentration, AuNP synthesis was completed within 14 h, whereas control protein extract took 24 h. Rate of AuNP synthesis increases with an increase in Au(III) ions in the growth medium and reached optimum values at 130 μM Au(III) (Supporting Information, Figure S7B). Further, Figure S7A showed that a sharp SPR band of AuNPs shifted from 535 nm to broad 545 nm in the case of AuNPs synthesized by protein extracted from mycelia grown in the presence 250–400 μM Au(III). As the SPR is known to be highly sensitive to nanoparticle size,[7,35] this suggests formation of larger AuNPs. TEM picture shows (Supporting Information, Figure S8) the formation of highly polydisperse, irregular AuNPs. Reduced protein activity might be responsible for uncontrolled growth of AuNPs. Inducible expressed proteins thus play a strong role in the Au biomineralization process and increases the nanoparticle synthesis rate.

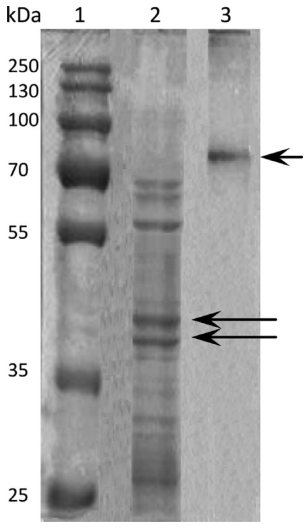

Figure 6. SDS-PAGE analysis of *R. oryzae* proteins responsible for gold biomineralization. Lane 2, unbound proteins after AuNP biosynthesis. Arrows indicate ~45 and ~42 kDa proteins. Lane 3, bound protein released from the AuNP surface after boiling with 1% SDS solution. Arrow indicates the ~80 kDa capping protein that determines AuNP stability.

This has significant practical importance in the scale-up of the AuNP biosynthetic process.

Role of Fungal Proteins. Fungal proteins responsible for AuNP synthesis were partially purified by separation of the membrane fraction from whole cell-free protein extract, followed by salted out using ammonium sulfate precipitation (experimental section in Supporting Information). UV–vis spectra after 12 h reaction showed that, among different fractions, 80% ammonium sulfate fraction had the highest AuNP biosynthetic activity based on nanoparticle synthesis rate and production yield (Supporting Information, Figure S9). Following biosynthesis using this fraction, unbound proteins were separated by centrifugation and subjected to SDS-PAGE (Figure 6). Electrophoresis showed a number of protein bands similar to those observed in the whole cell-free extract, including ~42 and ~45 kDa proteins, except the ~80 kDa protein that likely remained bound to the AuNP surface (Figure 6, lane 2). To confirm this observation, the AuNP-bound proteins were detached by boiling with 1% SDS solution for 10 min. The treated sample was further analyzed by SDS-PAGE, which showed the presence of a *ca.* ~80 kDa protein only (Figure 6, lane 3). Since SDS caused detachment of the bound proteins from the AuNP surface, it is likely that the ~80 kDa protein bound with the AuNP surface acted as a capping agent and confers stability to AuNPs, whereas ~42 and/or ~45 kDa proteins acted as reducing agents.

Our findings thus suggest that *R. oryzae* harbor several gold detoxification mechanisms to reduce Au(III) to Au^0 (AuNPs) (Figure 7). At this point, we do not have sufficient data to determine the sequence of

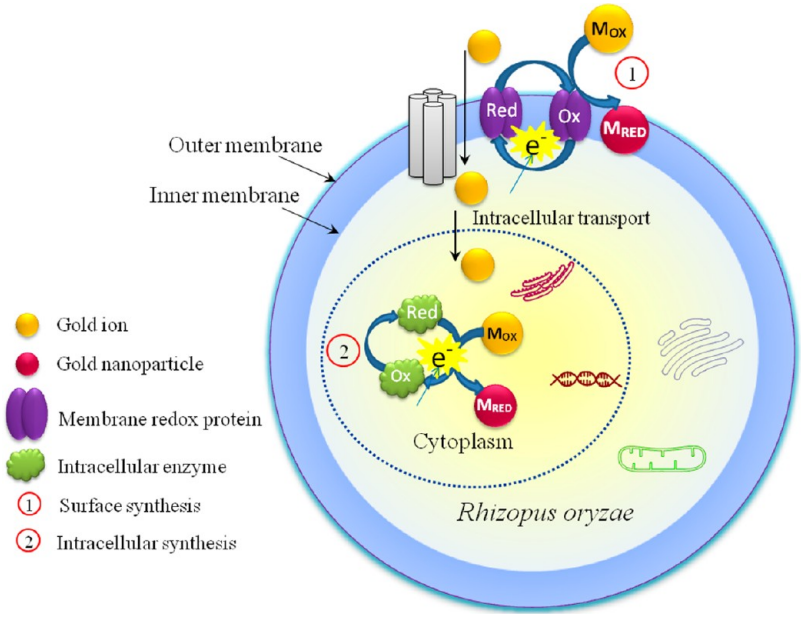

Figure 7. Proposed gold biomineralization mechanism in *R. oryzae*.

the Au biotransformation mechanism; however, at least two reduction routes took place: (a) binding of Au(III) on the cell wall through electrostatic interaction followed by reduction to AuNPs by proteins/enzyme present on the cell wall, and (b) diffusion or transportation of Au(III) into the cytoplasm and protein/enzymatic reduction to form AuNPs. The binding of Au(III) on the cell surface through electrostatic interaction and the appearance of Au^0 on the cell wall through intermediate Au(I) species formation were observed. Negatively charged gold ions bind on the positively charged *R. oryzae* mycelia through electrostatic interaction with phosphoprotein(s) and then become reduced to Au(I) species as a result of the high redox potential of Au(III) [*e.g.*, E_0 = 1.002 V for the reaction $AuCl_4^- + 3e^- = Au(s) + 4Cl^-$].[57] This led to a "grab" of electrons from suitable electron donors, resulting in reduction to Au(I) ions. The formation of Au(I) species was confirmed by the shift of C_{1s} and N_{1s} core-level peaks to higher energy in the XPS analysis and suggests the possibility of Au methylation as an additional detoxification mechanism.[50,51] Active mechanism was likely to be responsible for reduction of Au(I) species to metallic Au^0 particles as revealed from a protein induction experiment. Further, XPS confirmed that initial binding of Au(III) ions and subsequent reduction to Au(I) species occurs through a chemical interaction process, whereas reduction of Au(I) species to Au^0 occurs through a biochemically driven reduction pathway. Similar results were also obtained by X-ray absorption spectroscopy (XAS) in *Plectonema boryanum*, where Au(III) complexes get reduced to metallic Au through rapid (<2 min) formation of an intermediate Au(I)−S species and followed by a slower active reductive pathway to Au^0.[58]

The observation of Au^0 in the cytoplasmic space may be explained with the biochemically driven intracellular reduction that occurred through transportation of Au(III) from the cell wall into the cytoplasmic region where it was reduced by metal reductases to Au^0.[59] Since Au(I) species were observed also in the cytoplasm, it is likely that the cytoplasmic reduction of Au(III) to Au^0 occurs through the intermediate Au(I) species. Instead of electrostatic interaction, covalent binding was involved in the initial binding of Au(III) with cytoplasmic proteins as the latter carries negative ζ value. The whole protein analysis showed concentration-dependent up- and down-regulation of protein expression in the presence of different Au(III) concentrations. As mentioned previously, two up-regulated proteins of MW ~42 and ~45 kDa promoted AuNP biosynthesis, while the ~80 kDa protein bound with the AuNP surface and forms a stable gold bioconjugate system.

Conclusion. We characterize Au bioreduction process in viable *R. oryzae* to form AuNPs. Au(III) ions initially bind on the cell surface, then reduce to intermediate Au(I)−protein complexes and finally to AuNPs (Au^0). The majority of Au(III) are transported into the cytoplasmic region where they are reduced to AuNPs by cytoplasmic proteins, likely metal reductases. Growth of *R. oryzae* in the presence of sublethal Au(III) concentrations (130 μM) induces stress response proteins. At higher Au(III) concentrations (250 μM), Au toxicity results in damages to the cellular ultrastructure and AuNP biosynthesis is drastically reduced. The protein profile of the extract under sublethal dose [Au(III) < 130 μM] shows that two cytoplasmic proteins of ~45 and ~42 kDa are up-regulated and likely responsible for AuNP biosynthesis. The induction and/or suppression of proteins in response to sublethal Au(III)

concentration correlates with an increase in AuNP biosynthesis. Detachment of protein from AuNP bioconjugates shows that the ~80 kDa protein serves as a AuNP capping agent and stabilizes the bioconjugates through electrostatic repulsion, which impedes AuNP aggregation. Identification of Au-specific genetic responses may lead to the development of a low-cost AuNP biosynthesis process.

EXPERIMENTAL SECTION

Materials. Chloroauric acid ($HAuCl_4 \cdot 3H_2O$) and all chemicals were purchased from Sigma. Microbiological ingredients were obtained from Fluka. Ultrapure Millipore water (18.2 MΩ) was used in all AuNP biosynthesis experiments.

Synthesis of AuNPs by R. oryzae. Synthesis of AuNPs was carried out by incubating 0.2 g of fungal mycelia with 25 mL of $HAuCl_4$ (2 mM) solution in 50 mM phosphate buffer (pH 7.0). The mycelial suspension was incubated at 30 °C for 48 h under shaking (150 rpm), while bioreduction of chloroaurate ions ($AuCl_4^-$) was monitored by UV−vis spectroscopy measurement (Varian Cary 50 Bio, UK). Control experiments without fungal mycelia were also performed. The effect of pH on nanoparticle synthesis was carried out under identical conditions but varying the pH from 4.0 to 10.0. After 48 h, the mycelia were harvested by centrifugation at 10 000 rpm for 10 min, dried by lyophilization, and then dispersed in DI water. The dispersed solution was then analyzed by UV−vis spectroscopy. All of the experiments were performed in triplicate.

Synthesis of AuNPs by cell-free protein extract and partially purified proteins was carried out to determine the role of protein(s) in the reduction of gold ions. The experiments were performed as described above by incubating 2 mM $HAuCl_4$ solution in 50 mM phosphate buffer (pH 7.0) containing 100 μM NADH with 2 mg/mL protein extract. The nanoparticle formation was monitored by UV−vis spectroscopy.

The distribution, morphology, crystal structure, and chemical composition of as-synthesized AuNPs by the fungal mycelia and protein extract were characterized through SEM, TEM, and EDX analysis. The speciation and reduction mechanism of Au were carried out using high-performance XPS analysis. Particle size distribution and surface charge of AuNPs were measured through dynamic light scattering (DLS) measurement and zeta-potential analysis (Beckman Coulter Delsa Nano C, UK). The detailed experimental procedures are provided in the Supporting Information.

Metabolism of Gold by *R. oryzae*. The biochemical experiments were conducted to assess the response of *R. oryzae* to aqueous Au(III) ions and determine the possible mechanism of Au(III) detoxification. The experiments were carried out by growing *R. oryzae* in the presence of 10−400 μM gold, and mycelial weight and protein yield were then measured. The proteins were extracted from mycelia (as described in Supporting Information) grown in the presence of different concentrations of gold ions, and the expressions of proteins were visualized using 12% SDS-PAGE according to standard procedures. Electrophoresis was performed using the Bio-Rad Mini Protein gel system at a constant voltage of 90 V for 150 min against prestained molecular weight markers. Gels were stained with Coomassie Brilliant Blue R-250 solution.

The role of Au(III)-inducible expressed proteins in AuNP biosynthesis was studied to identify the Au biomineralization process and understand the Au-specific genetic responses in nanoparticle biosynthesis. The latter was carried as described above using cell-free and partially purified proteins extract from Au(III)-induced mycelia.

Identification of Proteins. After AuNP synthesis by partially purified protein, unbound proteins on AuNP surface were separated by centrifugation at 18 000 rpm for 30 min. The supernatant containing unbound proteins was collected and subjected to SDS-PAGE electrophoresis. The pellet containing nanoparticle-bound protein(s) was washed with phosphate buffer. The proteins bound with the nanoparticles were released from the nanoparticle surface by boiling with 1% SDS solution for 10 min. The supernatant was collected by centrifugation at 18 000 rpm for 15 min. The bound (SDS-treated) proteins were further analyzed by SDS-PAGE.

Further experimental details are provided in the Supporting Information.

Conflict of Interest: The authors declare no competing financial interest.

Acknowledgment. S.K.D. is supported by IRCSET-EMPOWER fellowship. SFI provides partial financial support (NAP Project N. 294). Ms. Suzanne Crotty (University College Cork) helped with TEM analysis, and BDI provided additional facility for AuNP characterization.

Supporting Information Available: Experimental details and additional results are provided in Supporting Information. This material is available free of charge *via* the Internet at http://pubs.acs.org.

REFERENCES AND NOTES

1. Tao, A. R.; Habas, S.; Yang, P. Shape Control of Colloidal Metal Nanocrystals. *Small* **2008**, *4*, 310–325.
2. Skrabalak, S. E.; Xi, Y. Pushing Nanocrystal Synthesis toward Nanomanufacturing. *ACS Nano* **2009**, *3*, 10–15.
3. Mafuné, F.; Kohno, J.; Takeda, Y.; Kondow, T. Formation of Gold Nanoparticles by Laser Ablation in Aqueous Solution of Surfactant. *J. Phys. Chem. B* **2001**, *105*, 5114–5120.
4. Sleytr, U. B.; Messner, P.; Pum, D.; Sara, M. Crystalline Bacterial Cell Surface Layers (S Layers): From Supramolecular Cell Structure to Biomimetics and Nanotechnology. *Angew. Chem., Int. Ed.* **1999**, *38*, 1034–1054.
5. Anstas, P. T.; Warner, J. C. *Green Chemistry: Theory and Practice*; Oxford University Press: New York, 1998.
6. Dahl, J. A.; Maddux, B. L. S.; Hutchison., J. E. Toward Greener Nanosynthesis. *Chem. Rev.* **2007**, *107*, 2228–2269.
7. Das, S. K.; Das, A. K.; Guha, A. K. Microbial Synthesis of Multishaped Gold Nanostructures. *Small* **2010**, *6*, 1012–1021.
8. Das, S. K.; Marsili, E. Bioinspired Metal Nanoparticle: Synthesis, Properties and Application. In *Nanomaterials*; Rahman, M. M., Ed.; InTech: Croatia, 2011; Chapter 11.
9. Cölfen, H. Biomineralization: A Crystal-Clear View. *Nat. Mater.* **2010**, *9*, 960–961.
10. Cölfen, H.; Mann, S. Higher-Order Organization by Mesoscale Self-Assembly and Transformation of Hybrid Nanostructures. *Angew. Chem., Int. Ed.* **2003**, *42*, 2350–2365.
11. Scheffel, A.; Gruska, M.; Faivre, D.; Linaroudis, A.; Plitzko, J. M.; Schüler, D. An Acidic Protein Aligns Magnetosomes along a Filamentous Structure in Magnetotactic Bacteria. *Nature* **2006**, *440*, 110–114.
12. Nam, K. T.; Lee, Y. J.; Krauland, E. M.; Kottmann, S. T.; Belcher, A. M. Peptide-Mediated Reduction of Silver Ions on Engineered Biological Scaffolds. *ACS Nano* **2008**, *2*, 1480–1486.
13. Doktycz, M. J.; Simpson, M. L. Nano-enabled Synthetic Biology. *Mol. Syst. Biol.* **2007**, *3*, 125.
14. Lovley, D. R.; Stolz, J. F.; Nord, G. L.; Phillips, E. J. P. Anaerobic Production of Magnetite by a Dissimilatory Iron-Reducing Microorganism. *Nature* **1987**, *330*, 252–254.
15. Southam, G.; Beveridge, T. J. The *In Vitro* Formation of Placer Gold by Bacteria. *Geochim. Cosmochim. Acta* **1994**, *58*, 4527–4530.
16. Lowe, C. R. Nanobiotechnology: The Fabrication and Applications of Chemical and Biological Nanostructures. *Curr. Opin. Struct. Biol.* **2000**, *10*, 428–434.
17. Bosecker, K. Bioleaching: Metal Solubilization by Microorganisms. *FEMS Microbiol. Rev.* **1997**, *20*, 591–604.

18. Chakraborty, N.; Banerjee, A.; Lahiri, S.; Panda, A.; Ghosh, A. N.; Pal, R. Biorecovery of Gold Using Cyanobacteria and an Eukaryotic Alga with Special Reference to Nanogold Formation—A Novel Phenomenon. *J. Appl. Phycol.* **2009**, *21*, 145–152.
19. Khalavka, Y.; Becker, J.; Sönnichsen, C. Synthesis of Rod-Shaped Gold Nanorattles with Improved Plasmon Sensitivity and Catalytic Activity. *J. Am. Chem. Soc.* **2009**, *131*, 1871–1875.
20. Tiwari, P. M.; Vig, K.; Dennis, V. A.; Singh, S. R. Functionalized Gold Nanoparticles and Their Biomedical Applications. *Nanomaterials* **2011**, *1*, 31–63.
21. Darbha, G. K.; Ray, A.; Ray, P. C. Gold Nanoparticle-Based Miniaturized Nanomaterial Surface Energy Transfer Probe for Rapid and Ultrasensitive Detection of Mercury in Soil, Water, and Fish. *ACS Nano* **2007**, *1*, 208–214.
22. Klaus, T.; Joerger, R.; Olsson, E.; Granqvist, C. G. Silver-Based Crystalline Nanoparticles, Microbially Fabricated. *Proc. Natl. Acad. Sci. U.S.A.* **1999**, *96*, 13611–13614.
23. Brown, S.; Sarikaya, M.; Johnson, E. A Genetic Analysis of Crystal Growth. *J. Mol. Biol.* **2000**, *299*, 725–735.
24. Lengke, M.; Fleet, M. E.; Southam, G. Morphology of Gold Nanoparticles Synthesized by Filamentous Cyanobacteria from Gold(I)−Thiosulfate and Gold(III)−Chloride Complexes. *Langmuir* **2006**, *22*, 2780–2787.
25. Das, S. K.; Marsili, E. A Green Chemical Approach for the Synthesis of Gold Nanoparticles: Characterization and Mechanistic Aspect. *Rev. Environ. Sci. Biotechnol.* **2010**, *9*, 199–204.
26. Du, L.; Xian, L.; Feng, J.-X. Rapid Extra-/Intracellular Biosynthesis of Gold Nanoparticles by the Fungus *Penicillium* sp. *J. Nanopart. Res.* **2011**, *13*, 921–930.
27. Kowshik, M.; Ashtaputre, S.; Kharrazi, S.; Vogel, W.; Urban, J.; Kulkarni, S. K.; Paknikar, K. M. Extracellular Synthesis of Silver Nanoparticles by a Silver-Tolerant Yeast Strain MKY3. *Nanotechnology* **2003**, *14*, 95.
28. Gericke, M.; Pinches, A. Microbial Production of Gold Nanoparticles. *Gold Bull.* **2006**, *39*, 22–28.
29. Avery, K. N.; Schaak, J. E.; Schaak, R. E. M13 Bacteriophage as a Biological Scaffold for Magnetically-Recoverable Metal Nanowire Catalysts: Combining Specific and Nonspecific Interactions To Design Multifunctional Nanocomposites. *Chem. Mater.* **2009**, *21*, 2176–2178.
30. Slocik, J. M.; Naik, R. R.; Stone, M. O.; Wright, D. W. J. Viral Templates for Gold Nanoparticle Synthesis. *Mater. Chem.* **2005**, *15*, 749–753.
31. Reith, F.; Etschmann, B.; Grosse, C.; Moors, H.; Benotmane, M. A.; Monsieurs, P.; Grass, G.; Doonan, C.; Vogt, S.; Lai, B.; *et al.* Mechanisms of Gold Biomineralization in the Bacterium *Cupriavidus metallidurans*. *Proc. Natl. Acad. Sci. U.S.A.* **2009**, *106*, 17757–17762.
32. Reith, F.; Rogers, S. L.; McPhail, D. C.; Webb, D. Biomineralization of Gold: Biofilms on Bacterioform Gold. *Science* **2006**, *313*, 233–236.
33. Narayanan, K. B.; Sakthivel, N. Biological Synthesis of Metal Nanoparticles by Microbes. *Adv. Colloid Interface Sci.* **2010**, *156*, 1–13.
34. Ban, K.; Kaieda, M.; Matsumoto, T.; Kondo, A.; Fukuda, H. Whole Cell Biocatalyst for Biodiesel Fuel Production Utilizing *Rhizopus oryzae* Cells Immobilized within Biomass Support Particles. *Biochem. Eng. J.* **2001**, *8*, 39–43.
35. Das, S. K.; Dickinson, C.; Lafir, F.; Brougham, D. F.; Marsili, E. Synthesis, Characterization and Catalytic Activity of Gold Nanoparticles Biosynthesized with *Rhizopus oryzae* Protein Extract. *Green Chem.* **2012**, *14*, 1322–1334.
36. Lloyd, J. R. Microbial Reduction of Metals and Radionuclides. *FEMS Microbiol. Rev.* **2003**, *27*, 411–425.
37. Shi, L.; Squier, T. C.; Zachara, J. M.; Fredrickson, J. K. Respiration of Metal (hydr)oxides by *Shewanella* and *Geobacter*: A Key Role for Multihaem c-Type Cytochromes. *Mol. Microbiol.* **2007**, *65*, 12–20.
38. Marsili, E.; Baron, D. B.; Shikhare, I.; Coursolle, D.; Gralnick, J. A.; Bond, D. R. *Shewanella* Secretes Flavins That Mediate Extracellular Electron Transfer. *Proc. Natl. Acad. Sci. U.S.A.* **2008**, *105*, 3968–3973.
39. Gadd, G. M. Microbial Metal Transformations. *J. Microbiol.* **2001**, *39*, 83–88.
40. Weiner, S.; Addadi, L. Crystallization Pathways in Biomineralization. *Annu. Rev. Mater. Res.* **2011**, *41*, 21–40.
41. Reith, F.; Lengke, M. F.; Falconer, D.; Craw, D.; Southam, G. The Geomicrobiology of Gold. *ISME J.* **2007**, *1*, 567–584.
42. He, S.; Guo, Z.; Zhang, Y.; Zhang, S.; Wang, J.; Gu, N. Biosynthesis of Gold Nanoparticles Using the Bacteria *Rhodopseudomonas capsulata*. *Mater. Lett.* **2007**, *61*, 3984–3987.
43. Scott, D.; Toney, M.; Muzikár, M. Harnessing the Mechanism of Glutathione Reductase for Synthesis of Active Site Bound Metallic Nanoparticles and Electrical Connection to Electrodes. *J. Am. Chem. Soc.* **2008**, *130*, 865–874.
44. Checa, S. K.; Espariz, M.; Audero, M. E.; Botta, P. E.; Spinelli, S. V.; Soncini, F. C. Bacterial Sensing of and Resistance to Gold Salts. *Mol. Microbiol.* **2007**, *63*, 1307–1318.
45. Mack, C.; Wilhelmi, B.; Duncan, J. R.; Burgess, J. E. Biosorption of Precious Metals. *Biotechnol. Adv.* **2007**, *25*, 264–271.
46. Das, S. K.; Das, A. K.; Guha, A. K. Adsorption Behavior of Rhodamine B on *Rhizopus oryzae* Biomass. *Langmuir* **2006**, *22*, 7265–7272.
47. Ahmad, A.; Senapati, S.; Khan, M. I.; Kumar, R.; Sastry, M. Extracellular Biosynthesis of Monodisperse Gold Nanoparticles by a Novel Extremophilic Actinomycete, *Thermomonospora* sp. *Langmuir* **2003**, *19*, 3550–3553.
48. Xie, J.; Zheng, Y.; Ying, J. Y. Protein-Directed Synthesis of Highly Fluorescent Gold Nanoclusters. *J. Am. Chem. Soc.* **2009**, *131*, 888–889.
49. Fadley, C. S.; Shirley, D. A. Electronic Densities of States from X-ray Photoelectron Spectroscopy. *J. Res. Natl. Bur. Stand., Sect. A* **1970**, *74*, 543–545.
50. Wackett, L. P.; Dodge, A. G.; Ellis, L. B. M. Microbial Genomics and the Periodic Table. *Appl. Environ. Microbiol.* **2004**, *70*, 647–655.
51. Bentley, R.; Chasteen, T. G. Microbial Methylation of Metalloids: Arsenic, Antimony, and Bismuth. *Microbiol. Mol. Biol. Rev.* **2002**, *66*, 250–271.
52. Yaganza, E.-S.; Danny, R.; Simard, M.; Arul, J.; Tweddell, R. L. Ultrastructural Alterations of *Erwinia carotovora* subsp. *atroseptica* Caused by Treatment with Aluminum Chloride and Sodium Metabisulfite. *Appl. Environ. Microbiol.* **2004**, *70*, 6800–6808.
53. Das, S. K.; Das, A. R.; Guha, A. K. A Study on the Adsorption Mechanism of Mercury on *Aspergillus versicolor* Biomass. *Environ. Sci. Technol.* **2007**, *41*, 8281–8287.
54. Monchy, S.; Benotmane, M. A.; Janssen, P.; Vallaeys, T.; Taghavi, S.; van der Lelie, D.; Mergeay, M. Plasmids pMOL28 and pMOL30 of *Cupriavidus metallidurans* Are Specialized in the Maximal Viable Response to Heavy Metals. *J. Bacteriol.* **2007**, *189*, 7417–7425.
55. Stoyanov, J. V.; Brown, N. L. The *Escherichia coli* Copper-Responsive *copA* Promoter Is Activated by Gold. *J. Biol. Chem.* **2003**, *278*, 1407–1410.
56. Pontel, L. B.; Audero, M. E; Espariz, M.; Checa, S. K.; Soncini, F. C. GolS Controls the Response to Gold by the Hierarchical Induction of *Salmonella*-Specific Genes That Include a CBA Efflux-Coding Operon. *Mol. Microbiol.* **2007**, *66*, 814–825.
57. Usher, A.; McPhail, D. C.; Brugger, J. A Spectrophotometric Study of Aqueous Au(III) Halide-Hydroxide Complexes at 25−80 °C. *Geochim. Cosmochim. Acta* **2009**, *73*, 3359–3380.
58. Lengke, M.; Ravel, B.; Fleet, M. E.; Wanger, G.; Gordon, R. A.; Gordon Southam, G. Mechanisms of Gold Bioaccumulation by Filamentous Cyanobacteria from Gold(III)-Chloride Complex. *Environ. Sci. Technol.* **2006**, *40*, 6304–6309.
59. Carney, C. K.; Harry, S. R.; Sewell, S. L.; Wright, D. W. Detoxification Biominerals. *Top. Curr. Chem.* **2007**, *270*, 155–185.